THE JOURNAL OF PHYSICAL CHEMISTRY B

Article

pubs.acs.org/JPCB

Molecular Simulation of the Thermophysical Properties of N-Functionalized Alkylimidazoles

C. Heath Turner,*[,†] Alex Cooper,[‡,§] Zhongtao Zhang,[†] Matthew S. Shannon,[†] and Jason E. Bara[†]

[†]Department of Chemical and Biological Engineering, and [‡]NSF-REU Site: Engineering Solutions for Clean Energy Generation, Storage and Consumption, Department of Chemical and Biological Engineering, University of Alabama, Tuscaloosa, Alabama 35487-0203, United States

[§]Department of Chemical Engineering, University of Virginia, Charlottesville, Virginia 22904-4741, United States

ABSTRACT: Molecular simulations are used to probe the thermophysical properties of a series of N-functionalized alkylimidazoles, ranging from *N*-methylimidazole to *N*-heptylimidazole. These compounds have been previously synthesized, and their solvation properties have been shown to be potentially useful for CO_2 capture from industrial sources. In this work, we use first-principles calculations to fit electrostatic charges to the molecular models, which are then used to perform a series of molecular dynamics simulations. Over a range of different temperatures, we benchmark the simulated densities and heat capacities against experimental measurements. Also, we predict the Henry's constants for CO_2 absorption and probe the solvents' structures using molecular simulation techniques, such as fractional free volume analysis and void distributions. We find that our simulations are able to closely reproduce the experimental benchmarks and add additional insight into the molecular structure of these fluids, with respect to their observed solvent properties.

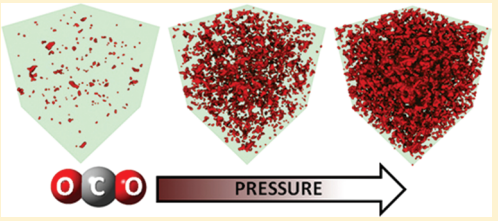

1. INTRODUCTION

There has been a great deal of recent experimental and computational research performed to identify promising solvents for CO_2 capture from industrial sources. For CO_2 capture, many studies have explored the technical and economic viability of ionic liquid (IL) compounds.[1,2] As the thermophysical properties of ILs are highly tunable, CO_2 can be selectively absorbed from a gas mixture, while their extremely low vapor pressures help minimize fugitive losses and improve the solvent regeneration efficiency. Compared to aqueous amine processes, which chemically absorb CO_2, the IL-based solvents tend to rely on physical absorption mechanisms. Due to the physical absorption mechanism, the energy demands for solvent regeneration can be reduced, which makes these compounds attractive for large-scale industrial applications, especially at higher concentrations/partial pressures of CO_2 (e.g., natural gas sweetening, precombustion CO_2 capture).

Although imidazolium-based ILs have demonstrated a great deal of potential as solvents for CO_2 capture, related compounds, namely, N-functionalized imidazoles (NFIs), have demonstrated similar performance characteristics in terms of CO_2 absorption as a function of pressure; however, NFIs possess much lower viscosities (1−2 orders of magnitude).[3] These NFI compounds are essentially neutral analogues to their IL counterparts, but they still retain the low volatility and favorable solvation properties associated with ILs. Although there have been many molecular simulation studies performed to characterize the thermophysical properties of imidazolium-based ILs, we instead focus on the molecular-level behavior of a series of alkylimidazoles, and we compare this behavior to recent experimental benchmarks available in the literature. Our simulation models are initially refined by using first-principles calculations to predict the partial charges on the imidazole groups, and then molecular dynamics simulations are used to predict the thermophysical properties of the bulk fluids. The alkyl chains vary in length from methyl (C_1) to heptyl (C_7), and we explore temperatures ranging from 293 to 353 K. We find that our newly parametrized models are able to closely reproduce the experimental benchmarks and add additional insight into the molecular structure of these fluids, with respect to their solvent properties. Although we only simulate pure fluid behavior, we expect to be able to use these models for simulating multicomponent systems, in order to help accelerate the rational development of designer solvents (or solvent mixtures) for industrial gas capture.

2. COMPUTATIONAL DETAILS

The molecular dynamics (MD) simulations were performed using the Gromacs 4.5.4 molecular dynamics software,[4] and the OPLS-AA force field[5] was used for describing the molecular interactions in the system. In order to accelerate the simulations, fixed bond lengths were imposed, and this mild constraint is expected to result in a negligible loss of accuracy, as demonstrated previously.[6−8] The initial configurations for the simulations were generated by placing 1000 randomly oriented molecules in a simulation box at a low density and

Received: March 28, 2012
Revised: May 16, 2012
Published: May 17, 2012

high temperature, followed by a series of simulations to compress the system to a liquid-like density at the desired temperature. Both canonical ensemble (NVT) simulations and isothermal−isobaric (NPT) simulations were performed, where the Nose−Hoover thermostat[9] was used to maintain the temperature, and in the case of the NPT simulations, the pressure was maintained with the Parrinello−Rahman barostat.[10,11] In the MD simulations, the equations of motion were integrated using the leapfrog method, with a time step of 0.002 ps, and after equilibration, the production phases were nominally conducted for a length of 1 ns. The site−site interactions were truncated at a distance of 1.4 nm, with standard tail corrections added to account for the long-range dispersion interactions,[12] and the particle mesh Ewald method[13] was used to capture the long-range electrostatic interactions.

In order to calculate Henry's constants, test particle insertions were performed with the TraPPE CO_2 interaction potential model of Potoff and Siepmann.[14] This model is a three-site model, with charge sites and Lennard-Jones sites centered on each atom location, and the bonds are fixed. Although other models are available, such as EPM2,[15] the TraPPE model has been effectively used for predicting CO_2 absorption in IL solvents in several recent simulation studies.[16−19] The cross-term interactions between the NFI molecules and CO_2 were approximated with the Lorentz−Berthelot mixing rules.

In developing the molecular models, we relied upon electronic structure calculations for assigning partial charges to the atom sites comprising the imidazole ring. The partial charges on the alkane tails remained fixed at their original OPLS values. The electronic structure calculations were performed by using first-principles density functional theory (DFT), as implemented in Gaussian 09,[20] in order to generate minimum energy configurations of the isolated molecules. These geometric optimizations were performed using the B3LYP functional[21,22] with the 6-31 g++(d,p) basis set. Following the geometry optimizations, the partial charges were calculated using a NBO population analysis[23] at the MP2/6-311 g++(3d,3p) level of theory.

3. RESULTS AND ANALYSIS

3.1. Density. In the process of refining the electrostatic charges in the MD simulations, the raw NBO charges on the imidazole rings (taken from the MP2 calculations) were proportionally scaled by a factor of 0.80. A value of 0.80 was used in order to improve the predicted densities, as compared to the experimental results.[3] Without the scaling, the simulated densities were all approximately 5−10% higher than the experimental values (perhaps due to the lack of polarizability in the molecular model). After the magnitude of the charges was scaled by a factor of 0.80, all of the simulated densities matched the experimental values within 1%. Regardless of the scaling, the general shapes of the density curves were unchanged, with respect to temperature. Although our species are nonionic, a similar level of scaling (0.80) was used by Liu and Maginn[24] and others[25] to scale the net ionic charges on their IL models. Also, others have scaled partial charges by similar values (0.75−0.90),[26] and they have found that this can help compensate for the lack of polarizability in fixed-charge models.

The resulting charges assigned to the atomic sites of our NFI models are shown in Table 1, and the corresponding site locations are illustrated in Figure 1. The charges on the imidazole rings were kept fixed at these values, regardless of the length of the alkane chain, which is consistent with the NBO charges predicted from our MP2 calculations. Although a close match to the experimental densities is beneficial, it is recognized that there can be inconsistencies when predicting other properties. For instance, matching experimental dielectric constants may be a reasonable route for generating more robust models, especially for the prediction of diffusion coefficients.[27]

Table 1. Partial Charge Assignments Corresponding to the NFI Molecular Models Used in the Molecular Dynamics Simulation Studies

site	species	charge (e^-)
	Imidazole Ring	
1	N	−0.392
2	N	−0.456
3	C	+0.248
4	H	+0.138
5	C	−0.024
6	H	+0.148
7	C	−0.040
8	H	+0.155
9	C	−0.049
10	H	+0.136
11	H	+0.136
	Alkane Tail	
12-end	C(−H_2)	−0.120
12-end	C(−H_3)	−0.180
12-end	−H	+0.060

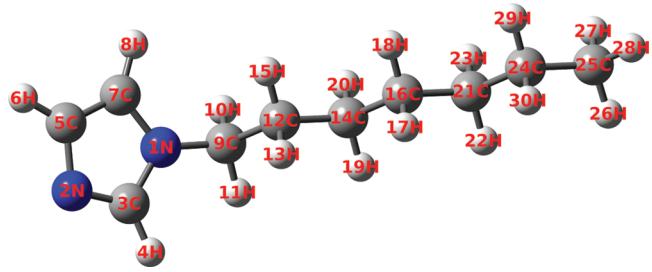

Figure 1. Generalized all-atom model of the NFI molecules, with numbers corresponding to the partial charge assignments shown in Table 1. Here, the heptyl NFI is used to illustrate the site labels. The dark gray atoms represent carbon, the blue atoms represent nitrogen, and the light gray atoms correspond to hydrogen.

The solvent density is a key property for designing industrial CO_2 removal processes, so it is an important aspect for us to consider. Furthermore, the solvent densities are correlated with the fractional free volume, which is an important criterion for CO_2 removal capacity. The comparisons between the computational and experimental densities are shown in Figure 2, where the experimental densities are taken from Shannon and Bara.[3] The statistical uncertainty of the simulation results are estimated by calculating block averages, resulting in a standard deviation of ±0.75 kg/m^3, and the experimental data is reported to be accurate to within ±0.05 kg/m^3. The experimental density for 1-heptylimidazole is linearly interpolated from the data for 1-hexylimidazole and 1-octylimidazole, in order to make comparisons with the simulations. Overall, the predicted densities of the NFI compounds are excellent, with errors of less than 1% over the temperature range of 293−353

dx.doi.org/10.1021/jp3029787 | J. Phys. Chem. B 2012, 116, 6529−6535

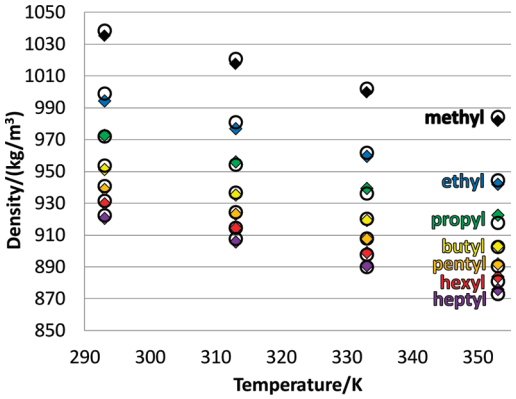

Figure 2. Simulated (hollow circles) and experimental (ref 3) (filled diamonds) densities of the NFI compounds at a pressure of 1 atm.

K. This agreement is encouraging, but it should be emphasized that the original parametrization resulted in simulated densities approximately 5−10% higher than those shown in Figure 2. We expect that the densities of other derivative species (based on an imidazole ring) may be able to benefit from our optimized partial charge assignments. In future work, we plan to test this parametrization to predict the performance of other functionalized imidazole compounds (e.g., 1,2-dialkylimidazoles), as well as mixtures.

3.2. Heat Capacity. The heat capacity data for our imidazole compounds were calculated from the simulated enthalpy versus temperature values, according to the expression $C_P = (\partial H/\partial T)_P$. Over the temperature range of our study (293−353 K), the enthalpy data followed a linear trend with respect to the temperature, with an R^2 value >0.995 for all fluids. Our predicted values of C_P are compared against experimental measurements,[28,29] as shown in Table 2.

Table 2. Comparison of Simulated (sim) and Experimental (Refs 28 and 29) (exptl) Heat Capacity Data of the NFI Compounds

alkyl group	C_P, sim [J/mol/K]	C_P, sim [J/g/K]	temp range, sim [K]	C_P, exptl [J/mol/K]	temp range, exptl [K]
methyl	220	2.67	293−353	154[a]	246−369
ethyl	264	2.75	293−353		
propyl	291	2.64	293−353	229.7	279−341
butyl	331	2.67	293−353		
pentyl	395	2.86	293−353	293.5	308−366
hexyl	434	2.85	293−353	325.4	309−363
heptyl	465	2.79	293−353	357.3	299−366

[a]The experimental heat capacity of methyl corresponds to a temperature of 333 K, calculated with the empirical fit reported by Verevkin et al. (ref 29).

According to the simulation results, the heat capacity is predicted to follow a linear trend, increasing from the *N*-methylimidazole to the *N*-heptylimidazole compound, which is a direct result of the increasing molecular weight of the fluids. When normalized by the molecular weights, all fluids are predicted to possess specific heat capacities of 2.64−2.86 J/g/K, which are somewhat higher than typical IL values (<2 J/g/K) and approximately 30% higher than the experimental values reported in Table 2. In terms of gas separation performance, lower heat capacities enhance the thermodynamic cycling efficiency of the fluid, as a larger fraction of the heat can be used to control the absorption/desorption of the gas. When considering the specific heat capacity, there is still a slight upward trend with respect to the length of the alkyl group, indicating that the shorter-chain alkyl imidazoles may possess a slight thermodynamic advantage in energy-intensive absorption processes.

3.3. Henry's Coefficient. In order to predict the adsorption behavior of CO_2 in our alkylimidazole compounds, we have implemented the Widom particle insertion method to calculate the excess chemical potential of CO_2 (μ^{ex}_{CO2}), over a range of temperatures. Similar to Elliott and co-workers, we prescreen the NFI solvents for void spaces, in order to increase the sampling efficiency of the particle insertions in our dense solvents. More sophisticated simulation approaches have been taken, as well, such as the continuous fractional component Monte Carlo (CFC MC) method described by Shi and Maginn,[17] and Kerle et al.[30] have used Bennett's overlapping distribution method. Comparisons of simulated Henry's constants of Shi and Maginn with low-pressure experimental results were found to be very good, and Kerle et al.'s comparisons with several experimental groups were also very consistent. Others[31] have used COSMO*therm* to make predictions of Henry's constants, and comparisons with 26 different ILs resulted in absolute average deviations of 15%. In general, the predictions with COSMO*therm*[32] were found to underestimate the experimental results, but not consistently. Recently, Vega et al.[33] have reviewed a number of different molecular-based approaches for predicting gas solubility in ILs, including an assessment of the predictive capability of these methods.

With our approach, the excess chemical potential of CO_2 can be calculated in the isothermal−isobaric ensemble by evaluating the expression[34]

$$\mu^{ex}_{CO_2} = \mu_{CO_2} - \mu^{ideal}_{CO_2} = -k_B T \ln\left(\frac{\langle V e^{-\beta\Delta U}\rangle}{\langle V\rangle}\right) \quad (1)$$

In eq 1, k_B is Boltzmann's constant, T is the absolute temperature, V is the volume, ΔU is the energy change of the test particle insertion, and β is the reciprocal of the product of the Boltzmann constant by the temperature. The chemical potential values are then used to estimate the Henry's constant of the CO_2, according to the expression

$$H = \rho RT \exp(\beta\mu^{ex,\infty}_{CO_2}) \quad (2)$$

In eq 2, ρ is the density, R is the gas constant, and ($\mu^{ex,\infty}_{CO2}$) corresponds to the chemical potential of CO_2 at infinite dilution in the NFI solvent. Henry's constants have previously been predicted using molecular simulations and compared against experiments, and simulations similar to ours were shown to underestimate the experimental values.[16] In addition to fundamental limitations of the molecular models, there are other possible reasons for the discrepancy. In our case, the experimental data[35] used to calculate the Henry's constants were taken at a CO_2 pressure of 4−5 atm, and this scenario (although relevant to chemical process engineering) is different from the simulated conditions, which correspond to the limit of infinite CO_2 dilution. Others have suggested that low-pressure measurements can reduce the experimental values by approximately 30%,[17] which in our cases would essentially close the gap between the experimental and simulated values. Regardless, we find consistent qualitative predictions of the Henry's constants of our NFI compounds, as a function of the

dx.doi.org/10.1021/jp3029787 | J. Phys. Chem. B 2012, 116, 6529−6535

Table 3. Comparison of Simulated (sim) and Experimental (Ref 35) (exptl) Henry's Constants for a Series of NFIs

	methyl			ethyl			butyl			hexyl		
T/K	sim[a]	exptl	% error	sim[a]	exptl	% error	sim[a]	exptl	% error	sim[a]	exptl	% error
293	75.0			76.5			49.8			46.2		
303	99.2	121.0	−18%	92.3	114.0	−19%	60.4	86.3	−30%	54.8	69.8	−21%
313	123.4			108.1			71.1			63.5		
318	140.1	180.0	−22%	118.1	153.0	−23%	78.0	123.0	−37%	68.3	98.3	−31%
333	190.1	221.0	−14%	148.0	180.0	−18%	98.6	150.0	−34%	82.5	118.0	−30%
348	211.8	254.0	−17%	177.1	201.0	−12%	121.9	170.0	−28%	97.1	134.0	−28%
353	219.0			186.8			129.7			102.0		

[a]The simulated results reported at 303, 318, and 348 K are interpolated from neighboring temperatures. The standard deviations of the simulated results all fall within ±10 bar, as calculated from five separate simulation runs.

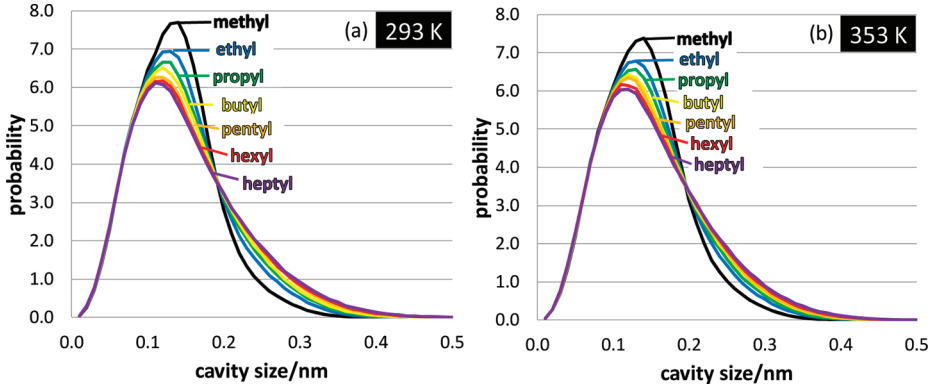

Figure 3. Cavity size distribution in the NFI solvents at (a) 293 and (b) 353 K.

alkyl chain length and as a function of temperature (Table 3). This provides reasonable justification for using such models for identifying CO_2-selective solvents.

3.4. Free Volume and Cavity Distribution. In order to further characterize the NFI solvent structure, cavity distributions of the fluid were calculated from the MD trajectories. The cavity distributions were estimated by choosing approximately 10^6 random points in the fluid (sampled from each of the molecular trajectories) and calculating the smallest distance to an NFI atom site. In these calculations, the distances are the site−site distances between the random sample sites and the center of the NFI atom sites. This is the same procedure used by Margulis to characterize the structure of imidazolium-based ILs.[36] It should be noted that this procedure neglects the radii of the solvent atoms. In order to approximate the available absorption space (in a static fluid), the net radii of the nearest-neighbor absorbent and absorbate atoms would need to be compared to the cavity size. Nonetheless, it is a useful approach for analyzing the changes in void structure among our different NFI molecules. In Figure 3, we show the cavity distribution of our fluids at two different temperatures (293 and 353 K).

As can be seen in Figure 3, there is a very clear trend in the cavity size distribution among the series of NFI solvents, and this trend is consistent at both the lower and higher temperature limits that were explored. In particular, it is evident that in the shorter-chain solvents (such as 1-methylimidazole) there is a distinct increase in the proportion of smaller cavities available (0.10−0.20 nm), whereas within the longer-chain solvents, there is a broader range of void spaces available, and at a size of 0.20 nm and beyond, the probability of observing larger voids increases with respect to chain length. The cavity sizes appear to correlate with the geometry of the molecules. For instance, the methyl-NFI molecules do not allow for larger pores to form, as there is enough flexibility and mobility to fill the larger voids. However, the longer-chain NFI molecules are less mobile and flexible, allowing larger voids to persist in the fluid, which can be relevant to the observed solvation properties.

A complementary view of the solvent structure can be obtained by analyzing the fractional free volume (FFV) of the solvent, which is equivalent to the expression $(V - V_o)/V$. In this expression, V is the total volume and V_o is the volume occupied by the NFI molecules. However, the term V_o cannot be rigorously defined, since the potential energy surface of a molecule is a smooth function (i.e., there is not a definitive method for identifying the surface boundary). Hence, it is important to distinguish between the total void volume versus the accessible void volume, which depends upon the nature of the solute. Our FFV analysis is based on a spherical solute (probe) molecule, and we calculate FFV as a function of the radius of our solute molecule. We treat the probe as a hard sphere and the solvent atoms as hard spheres, with radii corresponding to their Lennard-Jones parameters. With this approach, we periodically sample the configurations in our simulations by performing test particle insertions into the fluid. If there is no overlap between the randomly inserted particle and the solvent (corresponding to their hard-sphere radii), then there is a contribution to the void volume calculation. In Figure 4, we plot FFV versus solvent radius, in order to estimate the fraction of space available in our different NFI solvents with respect to solute size. Although this analysis does not account for the energetics of specific site−site interactions, it reveals information about the general fluid structure of our different solvents.

In Figure 4, only a few of the NFI compounds are included in the plot, due to the similarity in the results. The results at

dx.doi.org/10.1021/jp3029787 | J. Phys. Chem. B 2012, 116, 6529−6535

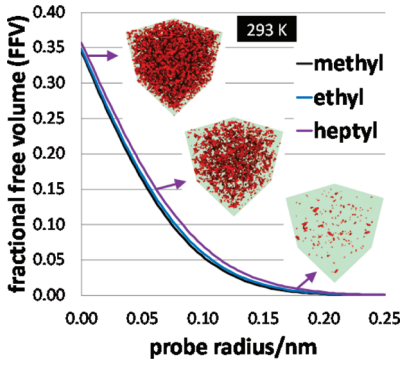

Figure 4. Fractional free volume as a function of the probe radius at 293 K. Snapshots representing the void space within the heptyl solvent are included for illustration.

higher temperatures are all very similar, as well. In general, the methyl and ethyl (shorter-chain) compounds have a lower FFV when the probe radius is small, and as the chain length is increased, the FFV quickly converges to a value that is approximately 10% higher than that of the 1-methylimidazole. However, it is interesting to examine the FFV accessible to the larger probes. In Figure 5, the data from Figure 4 are all

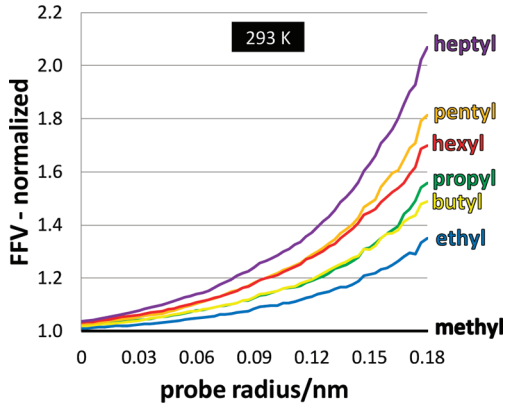

Figure 5. Fractional free volume as a function of the probe radius at 293 K, normalized with respect to the FFV of 1-methylimidazole.

normalized by the FFV of 1-methylimidazole. This clearly exposes the *relative* FFV of the solvents, particularly within the range of realistic probe radii, and this information is important for understanding their different absorption properties.

From Figure 5, it is clear that there is an increasing amount of larger voids in the longer-chain solvents, which may detract from the physical separation performance of these longer-chain solvents. For example, consider the kinetic diameters of CO_2 and CH_4, which are 0.330 and 0.382 nm, respectively.[37] In terms of physical interactions, it is more likely that CO_2 (radius of 0.165 nm) would become more selectively absorbed into the shorter-chain NFIs, whereas absorption of CH_4 (radius of 0.191 nm) would be more favorable in the longer-chain NFIs, as larger pores emerge in the fluid structure (reducing selectivity). Of course, the different molecular shapes, quadrupole moments, and van der Waals interactions will play important roles, as well. However, the trend of FFV versus absorption selectivity for the CO_2/CH_4 system is generally consistent with experimental observations. Figure 6 shows the experimentally predicted CO_2/CH_4 selectivity[35] as a function of the relative FFV values of the NFI solvents, corresponding to a probe

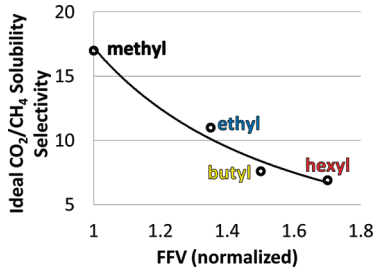

Figure 6. Selectivity of CO_2/CH_4 predicted from experiments (ref 35) vs the normalized FFV values, corresponding to a probe diameter of 0.18 nm (from Figure 5). The curve is a guide to the eye.

radius of 0.18 nm (as shown in Figure 5). This probe radius (0.18 nm) should indicate the accessible volume relevant to the selective adsorption of CO_2/CH_4, as the average kinetic radius of these two species is 0.178 nm. Although solute shape and site−site interactions are neglected in this analysis, accessible void space can be an important consideration when evaluating the physical absorption and separation of different sized solutes.

3.5. Radial Distribution Functions. We probed the local ordering of the NFI compounds by comparing site−site radial distribution functions as a function of the alkyl chain length at the lowest temperature, 293 K. Here, we explicitly examine the 2N:2N and 2N:3C distribution functions, which correspond to the site numbers shown in Figure 1. The resulting plots (Figure 7) reveal that the peak locations are very similar among the solvents, but there are definitely differences with respect to the peak heights, especially within the range of 0.4−0.8 nm. More specifically, the peak heights tend to increase, as the length of the alkyl chains increase. In general, this indicates an enhancement in the local order within these solvents, and this ordering behavior may be responsible for the presence of larger void spaces within the fluid (Figures 4 and 5). This local ordering may be affected by the chemical nature of the functional groups attached to the imidazole ring. Although we have only simulated alkyl chains, it is possible that alternative functional groups may affect the electronic structure of the imidazole rings, leading to shifts in the specific site−site interactions in the fluid. Shifts in the specific interactions may then induce physical reorganization of the fluid, leading to tunable void structures, and ultimately tunable solvation.

In Figure 7, there may be some head−tail ordering in the fluid (leading to increases in peak height with respect to tail length). Strong ordering behavior has been previously observed with other ionic liquid compounds.[38,39] However, since we are dealing with neutral molecules (versus the ionic liquids), the ordering is not expected to be as influential on the fluid structure.

4. CONCLUSIONS

Here, we have generated refined molecular models for predicting the thermophysical properties of N-functionalized alkylimidazoles (alkyl chain lengths ranging from C_1 to C_7). The new models are developed by refining the charge assignments on the imidazole rings, based on MP2 calculations of the isolated species. With these models, several direct comparisons are made with the experimental data available. The simulations demonstrate excellent agreement when comparing density values, and the predictions of the heat capacities and Henry's constants for CO_2 absorption are in very good qualitative agreement with the experiments.

dx.doi.org/10.1021/jp3029787 | J. Phys. Chem. B 2012, 116, 6529−6535

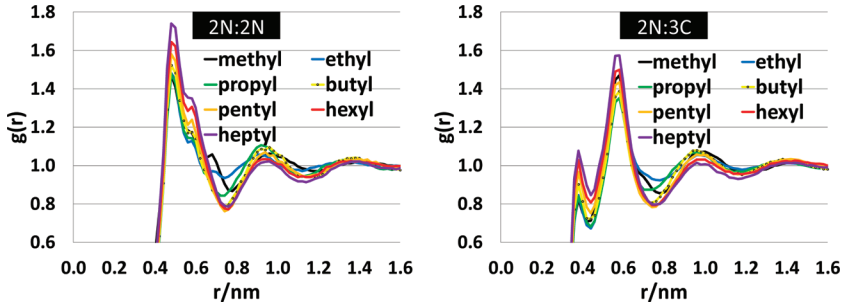

Figure 7. Site−site radial distribution functions at 293 K for (a) 2N:2N and (b) 2N:3C. The site labels correspond to those shown in Figure 1.

As these NFI solvents are potential candidates for industrial gas separation, via physical solvation, we explore the fluid structures of these solvents with analyses of the fractional free volume, cavity size distributions, and site−site radial distribution functions. The cavity size distributions and the fractional free volume of the solvents indicate that the shorter-chain imidazoles (methyl and ethyl) have smaller void spaces available for solvation. Moreover, there is a particularly strong distinction in the volumes available for absorption when examining the 0.36 nm diameter pores, relevant to the kinetic diameters of CO_2 and CH_4. There tends to be a correlation between the fluid structure and the CO_2/CH_4 selectivity of these fluids, and this insight may help direct investigations toward more selective solvents. Although we focus on many of the structural details of our NFI compounds, one cannot ignore the specific site−site interactions that also influence the solvation and selectivity. Also, our simulation studies are restricted to low solute loadings. As uptake increases, there can certainly be changes in the fluid structure, and this is an important aspect to explore in the future.

AUTHOR INFORMATION

Corresponding Author

*E-mail: hturner@eng.ua.edu. Phone: 205-348-1733.

Notes

The authors declare no competing financial interest.

ACKNOWLEDGMENTS

Support for this work provided by ION Engineering, LLC, United States Department of Energy—National Energy Technology Laboratory (DE-FE00005799), and partial support from the National Science Foundation Research Experiences for Undergraduates site program (EEC-1062705) and a CAREER award (CBET-0747690) are gratefully acknowledged.

REFERENCES

(1) Bara, J. E.; Carlisle, T. K.; Gabriel, C. J.; Camper, D.; Finotello, A.; Gin, D. L.; Noble, R. D. *Ind. Eng. Chem. Res.* **2009**, *48*, 2739.
(2) Bara, J. E.; Camper, D. E.; Gin, D. L.; Noble, R. D. *Acc. Chem. Res.* **2010**, *43*, 152.
(3) Shannon, M. S.; Bara, J. E. *Ind. Eng. Chem. Res.* **2011**, *50*, 8665.
(4) Hess, B.; Kutzner, C.; van der Spoel, D.; Lindahl, E. *J. Chem. Theory Comput.* **2008**, *4*, 435.
(5) Jorgensen, W. L.; Maxwell, D. S.; TiradoRives, J. *J. Am. Chem. Soc.* **1996**, *118*, 11225.
(6) Shim, Y.; Choi, M. Y.; Kim, H. J. *J. Chem. Phys.* **2005**, 122.
(7) Morrow, T. I.; Maginn, E. J. *J. Phys. Chem. B* **2002**, *106*, 12807.
(8) Hanke, C. G.; Price, S. L.; Lynden-Bell, R. M. *Mol. Phys.* **2001**, *99*, 801.
(9) Hoover, W. G. *Phys. Rev. A* **1985**, *31*, 1695.
(10) Parrinello, M.; Rahman, A. *Phys. Rev. Lett.* **1980**, *45*, 1196.
(11) Parrinello, M.; Rahman, A. *J. Appl. Phys.* **1981**, *52*, 7182.
(12) Allen, M. P.; Tildesley, D. J. *Computer Simulation of Liquids*; Oxford University Press: Oxford, U.K., 1989.
(13) Essmann, U.; Perera, L.; Berkowitz, M. L.; Darden, T.; Lee, H.; Pedersen, L. G. *J. Chem. Phys.* **1995**, *103*, 8577.
(14) Potoff, J. J.; Siepmann, J. I. *AIChE J.* **2001**, *47*, 1676.
(15) Harris, J. G.; Yung, K. H. *J. Phys. Chem.* **1995**, *99*, 12021.
(16) Ghobadi, A. F.; Taghikhani, V.; Elliottt, J. R. *J. Phys. Chem. B* **2011**, *115*, 13599.
(17) Shi, W.; Maginn, E. J. *J. Phys. Chem. B* **2008**, *112*, 2045.
(18) Aparicio, S.; Atilhan, M.; Khraisheh, M.; Alcalde, R.; Fernandez, J. *J. Phys. Chem. B* **2011**, *115*, 12487.
(19) Perez-Blanco, M. E.; Maginn, E. J. *J. Phys. Chem. B* **2011**, *115*, 10488.
(20) Frisch, M. J.; Trucks, G. W.; Schlegel, H. B.; Scuseria, G. E.; Robb, M. A.; Cheeseman, J. R.; Scalmani, G.; Barone, V.; Mennucci, B.; Petersson, G. A.; Nakatsuji, H.; Caricato, M.; Li, X.; Hratchian, H. P.; Izmaylov, A. F.; Bloino, J.; Zheng, G.; Sonnenberg, J. L.; Hada, M.; Ehara, M.; Toyota, K.; Fukuda, R.; Hasegawa, J.; Ishida, M.; Nakajima, T.; Honda, Y.; Kitao, O.; Nakai, H.; Vreven, T.; Montgomery, J. A., Jr.; Peralta, J. E.; Ogliaro, F.; Bearpark, M.; Heyd, J. J.; Brothers, E.; Kudin, K. N.; Staroverov, V. N.; Kobayashi, R.; Normand, J.; Raghavachari, K.; Rendell, A.; Burant, J. C.; Iyengar, S. S.; Tomasi, J.; Cossi, M.; Rega, N.; Millam, J. M.; Klene, M.; Knox, J. E.; Cross, J. B.; Bakken, V.; Adamo, C.; Jaramillo, J.; Gomperts, R.; Stratmann, R. E.; Yazyev, O.; Austin, A. J.; Cammi, R.; Pomelli, C.; Ochterski, J. W.; Martin, R. L.; Morokuma, K.; Zakrzewski, V. G.; Voth, G. A.; Salvador, P.; Dannenberg, J. J.; Dapprich, S.; Daniels, A. D.; Farkas, Ö.; Foresman, J. B.; Ortiz, J. V.; Cioslowski, J.; Fox, D. J. *Gaussian 09*, revision A.1; Gaussian Inc.: Wallingford, CT, 2009.
(21) Becke, A. D. *J. Chem. Phys.* **1993**, *98*, 5648.
(22) Lee, C. T.; Yang, W. T.; Parr, R. G. *Phys. Rev. B* **1988**, *37*, 785.
(23) Reed, A. E.; Curtiss, L. A.; Weinhold, F. *Chem. Rev.* **1988**, *88*, 899.
(24) Liu, H.; Maginn, E. *J. Chem. Phys.* **2011**, 135.
(25) Bhargava, B. L.; Balasubramanian, S. *J. Chem. Phys.* **2007**, 127.
(26) Schroeder, C. *Phys. Chem. Chem. Phys.* **2012**, *14*, 3089.
(27) Fennell, C. J.; Li, L.; Dill, K. A. *J. Phys. Chem. B* [Online early access]. DOI: 10.1021/jp3002383. Published Online: March 7, **2012**. http://pubs.acs.org/doi/abs/10.1021/jp3002383.
(28) Emel'yanenko, V. N.; Portnova, S. V.; Verevkin, S. P.; Skrzypczak, A.; Schubert, T. *J. Chem. Thermodyn.* **2011**, *43*, 1500.
(29) Verevkin, S. P.; Zaitsau, D. H.; Emel'yanenko, V. N.; Paulechka, Y. U.; Blokhin, A. V.; Bazyleva, A. B.; Kabo, G. J. *J. Phys. Chem. B* **2011**, *115*, 4404.
(30) Kerle, D.; Ludwig, R.; Geiger, A.; Paschek, D. *J. Phys. Chem. B* **2009**, *113*, 12727.
(31) Sumon, K. Z.; Henni, A. *Fluid Phase Equilib.* **2011**, *310*, 39.
(32) Eckert, F.; Klamt, A. *COSMOtherm*; C2.1, release 01.08; Cosmologic GmbH & Co.: Leverkusen, Germany, 2006.
(33) Vega, L. F.; Vilaseca, O.; Llovell, F.; Andreu, J. S. *Fluid Phase Equilib.* **2010**, *294*, 15.
(34) Frenkel, D.; Smit, B. *Understanding Molecular Simulations: from Algorithms to Applications*; Academic Press: San Diego, CA, 2002.

(35) Shannon, M. S.; Tedstone, J. M.; Danielsen, S. P. O.; Bara, J. E. *Ind. Eng. Chem. Res.* **2012**, *51*, 515.
(36) Margulis, C. J. *Mol. Phys.* **2004**, *102*, 829.
(37) Sircar, S. *Ind. Eng. Chem. Res.* **2006**, *45*, 5435.
(38) Wang, Y. T.; Voth, G. A. *J. Am. Chem. Soc.* **2005**, *127*, 12192.
(39) Lopes, J. N. C.; Gomes, M. F. C.; Padua, A. A. H. *J. Phys. Chem. B* **2006**, *110*, 16816.